Assessment of Different Topographic Corrections in Landsat-TM Data for Mapping Vegetation Types

David Riaño, Emilio Chuvieco, Javier Salas, and Inmaculada Aguado

***Abstract*—Different methods for topographic correction of Landsat Thematic Mapper images have been assessed in the context of mapping vegetation types. The best results were obtained with a variation of the C method, which takes into account the overcorrection of low illuminated slopes by the original C method. The performance of this method was tested using two criteria: the changes in the spectral characteristics of the image and the reduction in standard deviation of each vegetation type after the correction.**

***Index Terms*—Landsat Thematic Mapper (TM), topographic correction, vegetation mapping.**

I. Relevance of Topographic Correction for Vegetation Mapping

The item *topographic correction,* or *topographic normalization,* refers to the compensation of the different solar illuminations due to the irregular shape of the terrain. This effect causes a high variation in the reflectance response for similar vegetation types: shaded areas show less than expected reflectance, whereas in sunny areas the effect is the opposite (Fig. 1). Therefore, the process of topographic normalization may be critical in areas of rough terrain, as a preliminary step to the multispectral and for multitemporal digital classification of vegetation types. This correction has been acknowledge in the literature [2]–[4], although some authors have indirectly approached reflectance variations caused by topographic effects by including digital terrain models as ancillary variables in multiband classification [5]–[7].

Although this approach has yielded acceptable results, a more refined topographic correction should reduce the internal variability of each vegetation type, since the corrected reflectance is more related to the geometrical or biological properties of the plant than the original reflectance even when considering its terrain location.

Manuscript received April 25, 2002; revised January 30, 2003. This research was supported by the Spanish Ministry of Science through project number AGF96-2094-CE. The Autonomous Region of Madrid (Spain) and a Fulbright Grant with the financial sponsorship of the Spanish Ministry of Education, Culture & Sports supported D. Riaño for this study.

D. Riaño was with the Department of Geography, University of Alcalá, Madrid, Spain. He is now with the Center for Spatial Technologies and Remote Sensing, Department of Land, Air and Water Resources, University of California, Davis, CA 95616-8617 USA (e-mail: driano@ucdavis.edu).

E. Chuvieco, J. Salas, and I. Aguado are with the Department of Geography, University of Alcalá, Madrid 28801 Spain (e-mail: emilio.chuvieco@uah.es; javier.salas@uah.es; inmaculada.aguado@uah.es).

Digital Object Identifier 10.1109/TGRS.2003.811693

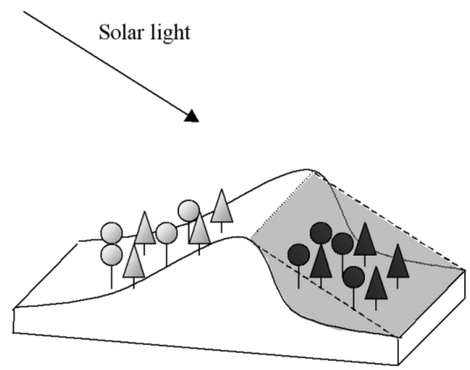

Fig. 1. Effect of topography on reflectance [25].

The main difficulty in applying topographic corrections is related to the lack of standard and generally accepted models. A wide variety of methods have been proposed in the literature (see Section II); however, there is no clear consensus on methods that may be universally applicable. Additionally, the availability of digital terrain models has, until recently, been restricted to highly developed countries, therefore precluding the general application of topographic normalization. The growing availability of global digital terrain datasets, such as those derived from the interferometric shuttle mission (*http://www.fas.org/irp/program/collect/ifsar.htm*) will help to solve this limitation.

II. Review of Topographic Normalization Methods

As it is well known, raw digital values (DVs) derived from satellite optical systems cannot confidently be used for geophysical measurements and multitemporal studies, since they include effects derived from sensor calibration, as well as atmospheric and topographic interferences. Calibration values to transform DV to sensor radiance are typically provided in the image metadata, and therefore the user needs only to compensate for atmospheric and topographic effects. The model to obtain true reflectance from sensor radiance may be expressed as

$$\rho_k = \frac{K\pi\left(\dfrac{(L_{\mathrm{sen},k} - L_{a,k})}{\tau_{k,o}}\right)}{E_{o,k}\cos\theta_z \tau_{k,i} + E_{d,k}} \quad (1)$$

where K is a correction factor of the annual variations of earth-sun distance, computed from Julian day; $L_{\mathrm{sen},k}$, is the sensor radiance in band k; $L_{a,k}$ the atmospheric upwelling radiance scattered at the sensor for the same band; $\tau_{k,o}$ and $\tau_{k,i}$ are the path atmospheric transmittances of the upwelling (ground surface–sensor path) and downwelling (sun–ground surface path) flows, respectively; $E_{0.k}$ is the solar irradiance at the top of the atmosphere; θ_z is the sun zenith angle; and $E_{d,k}$ the diffuse irradiance at the surface.

Topographic correction should affect the denominator parameters, since changing illumination conditions affect the actual solar irradiance received at a single pixel. Some authors recommend applying atmospheric correction prior to the topographic normalization [8], [9], while others recommend that they be applied concurrently [10], [11]. Here, we will distinguish between the two steps, focusing on the topographic correction.

Methods for correcting the topographic effect may be grouped into two categories: those based on band ratios, and those requiring digital elevation models (DEMs). The former are much simpler and do not require additional input data. The reflectance is assumed to increase or decrease proportionally in the two ratio bands. Therefore, the quotient between them will compensate for topographic effects [12], [13]. This assumption is valid for the incident angles, which are wavelength independent, but not for the diffuse irradiance, which changes in each spectral band [3], [14]. An additional problem is the loss of spectral resolution when ratios are used, which is a drawback in multispectral classification.

The second group of topographic correction methods based on modeling illumination (IL) conditions and require a DEM of the same resolution as the image to be corrected. The DEM is required to compute the incident angle (γ_i), defined as the angle between the normal to the ground and the sun rays [15] (Fig. 2). The IL parameter varies from -1 (minimum) to $+1$ (maximum illumination) and may be computed as follows:

$$\mathrm{IL} = \cos\gamma_i = \cos\theta_p \cos\theta_z + \sin\theta_p \sin\theta_z \cos(\phi_a - \phi_o) \quad (2)$$

where θ_p is the slope angle; θ_z is the solar zenith angle; ϕ_a is the solar azimuth angle; and ϕ_o is the aspect angle. Once IL is computed for the whole image, the flat-normalized reflectance of each pixel is estimated using different methods. They can be grouped into two categories: Lambertian and non-Lambertian, depending on whether they assume that reflectance is independent of observation and incident angles or not.

A. Lambertian Methods

From the proposed Lambertian methods, the most widely used is the cosine method, proposed by Teillet *et al.* [1], and later modified by Civco [15]. It is computed as

$$\rho_H = \rho_T \left(\frac{\cos\theta_z}{\mathrm{IL}}\right) \quad (3)$$

where ρ_H is the reflectance of a horizontal surface; ρ_T is the reflectance of an inclined surface. The method assumes that the lower the IL, the higher is the corrected reflectance. Additionally, the sun zenith angle is used to take into account nonverticality of sun rays.

Several authors have shown that this method overcorrects the image, mainly in areas of low IL [2], [9], [16]. An improved version has been proposed by Civco [15], which considers the average IL conditions

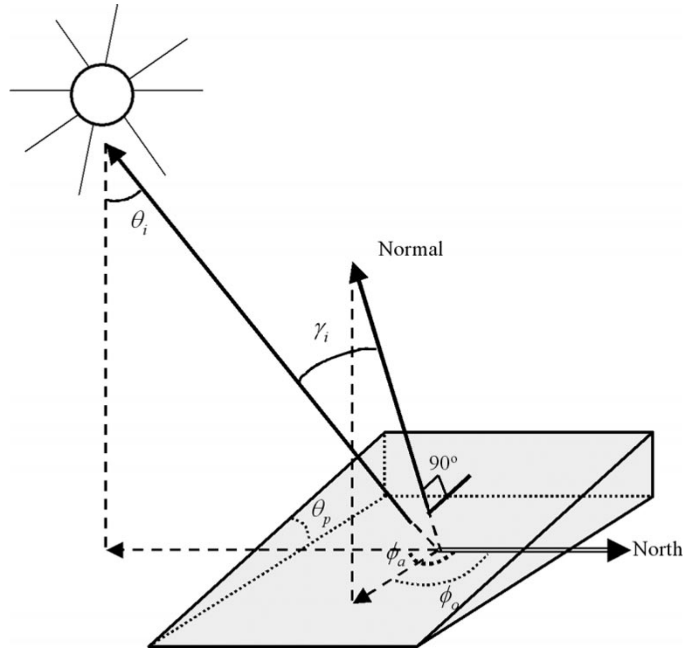

Fig. 2. Angles involved in the computation of the IL.

$$\rho_H = \rho_T + \left[\rho_T \left(\frac{\mathrm{IL}_m - \mathrm{IL}}{\mathrm{IL}_m}\right)\right] \quad (4)$$

where IL_m is the average IL value of the study area.

These models are wavelength independent, since the correction is based on the same factor for all the bands. As said before, this assumption is not appropriate as far as diffuse irradiance concerns. Therefore, it should be more appropriate to propose band-dependent factors of correction.

B. Non-Lambertian Methods

The Lambertian assumption is very convenient to simplify procedures but unrealistic, since most covers are rugged, having a non-Lambertian behavior. The bidirectional reflectance distribution function (BRDF) describes how reflectance varies in each cover considering the angles of incidence and observation [3], [17]. The determination of BRDF is rather complex, since it describes the reflectance behavior at all possible angles of incidence, combined with all possible angles of reflection [18]. Therefore, sometimes it is more convenient to assume a Lambertian surface than introducing a model that does not comply with the non-Lambertian properties of the surface.

The main methods are based on the ideas of Minnaert [19], who first proposed a semiempirical equation to assess the roughness of the moon's surface

$$\rho_H = \rho_T \left(\frac{\cos\theta_z}{\mathrm{IL}}\right)^{K_k} \quad (5)$$

where K_k is the Minnaert constant for band k. The term K models the non-Lambertian behavior. If $K = 1$, the surface behaves as a perfect Lambertian reflector. It is necessary to calculate the value of K for each band before performing the correction, by linearization of the previous equation

$$\ln(\rho_T) = \ln(\rho_H) + K_k \ln\left(\frac{\mathrm{IL}}{\cos\theta_z}\right). \quad (6)$$

This can be done with an ordinary linear regression, where K_k and $\ln(\rho_H)$ are the regression coefficients. That is, ρ_H is constant for the entire image.

This equation was further modified to include the slope of the terrain [12]

$$\rho_H = \rho_T \cos\theta_p \left(\frac{\cos\theta_z}{\mathrm{IL}\cos\theta_p}\right)^{K_k}. \quad (7)$$

Some authors suggest modeling the slope separately [10], to reduce noise inherent to the topographic correction, reducing thereby its effectiveness [8].

Another method is the empirical–statistical method of Teillet [1] that assumes a linear correlation between the reflectance of each band and IL

$$\rho_T = \rho_H + m_k\,\mathrm{IL} \quad (8)$$

where m_k is the slope of the regression line for band k. The ρ_H is considered constant for the entire image, being the intercept in the regression equation.

A variation of this empirical approach is named the C correction [1], defined as

$$\rho_H = \rho_T \left(\frac{\cos\theta_z + c_k}{\mathrm{IL} + c_k}\right) \quad (9)$$

where $c_k = b_k/m_k$, for $\rho_T = b_k + m_k$ IL. Therefore, it is based on the empirical–statistical approach [see (8)].

This model introduces a parameter c_k that is the quotient between the gradient (b_k) and intercept (m_k) of the regression equation, ρ_T versus IL.

The main objective of this study was to test different methodologies for topographic correction of Landsat Thematic Mapper (TM) images in mapping vegetation types. The performance of each method will be assessed by two ways: 1) how they preserve the original spectral structure of the image and 2) how they increase the statistical homogeneity of each target category, hence reducing the reflectance changes caused by different illumination conditions.

III. Methodology

A. Study Area

Cabañeros National Park is located about 200 km south of Madrid on the western area of Spain's southern plateau and occupies an area of around 41 000 ha. It forms a portion of the southern limit of the *Montes de Toledo*, which comprise a series of small mountain ranges or "sierras" trending in a NW–SE direction. Elevations vary from around 900–1400 m along the sierra ridges, to about 500–700 m at the foot of the valleys. The park's main features consist of a series of Paleozoic ranges intermingled with plioquaternary conglomerates or "rañas," which are flat wide plains formed of eroded quartzite pebbles from the surrounding sierras. Cabañeros is one of the best examples of Iberian–Mediterranean forest. The park's main forest species, in order of importance and abundance, are holm oak (*Quercus ilex*), cork oak (*Q. suber*), and gall oak (*Q. faginea*). The distribution and density of trees varies greatly according to terrain, temperature, and humidity. In the flat low areas, grasslands are mixed with scattered holm oaks. In the steeper more mountainous areas, oak woods with *Q. faginea* and *Q. pyrenaica* are found in colder damper climates at the mesomediterranean vegetation level. Degraded areas are dominated by heliophilae species, mainly rock roses (*Cistus ladanifer*, *C. populifolius*) and heather (*Erica australis*, *E. umbellata* and *E. arborea*) [20].

B. Dataset

This study is based on a summer quarter Landsat-TM scene (July 21, 1997). The image is cloud free and has good illumination conditions (high sun elevation angle), which minimizes the topographic distortion. Winter images had a high topographic distortion where steep areas are fully shaded. Additionally, a vegetation map produced by the forest guards of Cabañeros National Park using aerial photography and extensive fieldwork was available. The map has 107 vegetation classes. Finally, the DEM is generated from digitised contour lines from a 1:50.000 scale map (contours every 20 m) as described below.

C. Geometric Correction

The quarter of Landsat-TM scene was orthorectified using a set of 40 ground control points (GCPs) extracted from 1:50.000 scale maps and the DEM. The error of the model was under half a pixel ($x = 0.43$, $y = 0.38$). The nearest neighbor resampling method was used.

D. Atmospheric Correction

Atmospheric correction was based on the default transmittance method proposed by Chavez [21], which recommends standard down-welling transmittance values. Values for bands TM1 to TM4 were taken from Chavez [21] ($\tau_{k,i} = 0.70$, 0.78, 0.85, and 0.91, respectively). This author assumes full transmittance for TM5 and TM7 bands, but we preferred to be more cautious and took the values proposed by Gilabert *et al.* [22] ($\tau_{k,i} = 0.95$ and 0.97, respectively), whose study area had similar atmospheric conditions to our site. We used the original method [21] for the other variables, i.e., $L_{a,k}$ equal to the DV of the dark-object on each band; $\tau_{k,o}$ equal to one; and it is ignored $E_{d,k}$.

E. Generation of DEM

A DEM of the area was generated by spatial interpolation of digitised contour lines from a 1:50.000 scale map (contour lines every 20 m), using the distance transform algorithm [23]. Elevation data was only produced within the park and the surrounding areas (Fig. 3).

The DEM was validated using an independent source: a differential GPS with dual frequency (L1/L2). A total of 123 elevation points were measured in the study area covering the entire National Park. The mean squared error of the DEM, based on these independent x, y, and z points, was 9.78 m, which is appropriate for correcting 30-m resolution TM images.

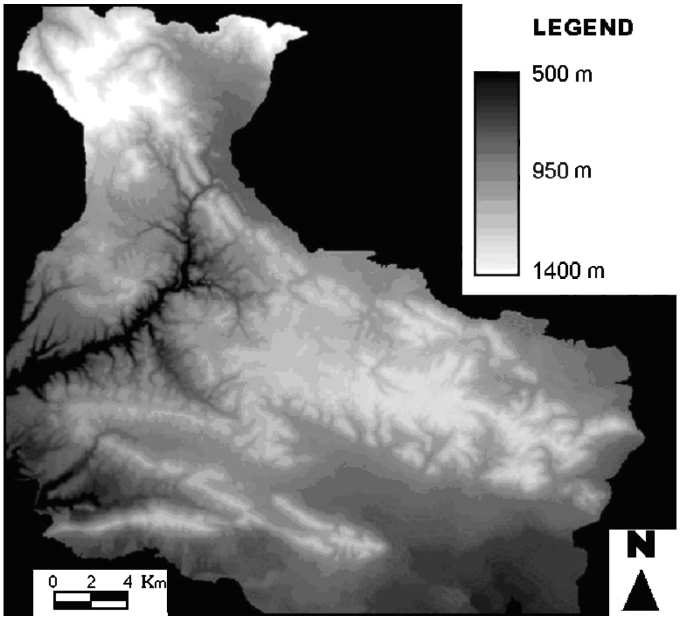

Fig. 3. DEM generated from contour lines.

The DEM was used to generate the slope and IL map. The slope computed at each pixel is the plane formed by the vector connecting the left and right neighbors versus the vector connecting the upper and lower neighbors of the pixel. The IL of each pixel was computed considering the solar zenith and azimuth angles when the Landsat-TM image was acquired, as well as the slope and the aspect of each pixel.

F. Topographic Corrections Tested

The performance of the following algorithms for topographic corrections were tested: the IL weighted by the IL_m [(4)], the Minnaert method [including the slope: (7)], the C-correction [(9)] and a variation of this method, based on a smoothed IL value.

Most methods produce an overcorrection in those pixels where IL is low. Therefore, a variation in the calculation of the IL was carried out, by smoothing the original slope. Considering average slopes in roughest sections of the study area, a smoothing factor of 3, 5, and 7 was tested (Fig. 4). Initially we have

$$\theta_p = \arctan\left(\frac{b}{a}\right) \tag{10}$$

which is then transformed into

$$\theta_p' = \arctan\left(\frac{b}{X * a}\right) \tag{11}$$

where $X = 3, 5,$ or 7.

There are several possible methods to assess the results of the topographic corrections. First, the analysis of changes in the spectral characteristics of the image after correction [15]. Ideally these changes should be low; otherwise it would imply an under- or overcorrection. A second criteria would be based on the graphical analysis of ρ_T and ρ_H versus IL for each cover

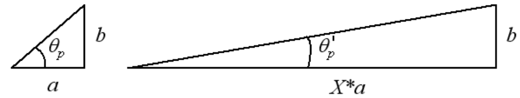

Fig. 4. Smoothed slope to calculate IL.

TABLE I
MEAN AND SD DIFFERENCE, IN PERCENT REFLECTANCE, BETWEEN THE ATMOSPHERICALLY CORRECTED DATA AND EACH TOPOGRAPHIC CORRECTION FOR EACH TM BAND AND ALSO FOR THE TOTAL SUM OF ALL BANDS

		TM1	TM2	TM3	TM4	TM5	TM7	Total change
IL weigh.	Mean	0.02	0.04	0.06	0.04	0.16	0.14	0.47
	SD	0.04	0.06	0.09	-0.09	0.30	0.23	0.64
Minnaert	Mean	-0.15	-0.17	-0.21	0.13	-0.67	-0.69	-1.76
	SD	-0.04	-0.03	-0.01	0.08	0.17	0.08	0.25
C-correction	Mean	-0.08	-0.13	-0.17	-0.12	-0.45	-0.39	-1.34
	SD	-0.03	-0.08	-0.08	0.00	0.17	0.10	0.08
C-correction-3	Mean	-0.02	-0.04	-0.04	-0.07	-0.16	-0.12	-0.46
	SD	0.00	0.00	0.00	0.02	0.10	0.05	0.17
C-correction-5	Mean	-0.02	-0.03	-0.04	-0.09	-0.16	-0.13	-0.48
	SD	-0.01	-0.01	-0.02	0.03	0.07	0.02	0.08
C-correction-7	Mean	-0.03	-0.04	-0.05	-0.10	-0.19	-0.15	-0.56
	SD	-0.01	-0.02	-0.03	0.02	0.05	0.01	0.02

TABLE II
DESCRIPTION OF THE VEGETATION CLASSES USED TO ANALYZE THE RESULTS OF EACH TOPOGRAPHIC CORRECTION

Class	Vegetation	Density	Main species
1	Shrub	**High**	*Erica australis, Cistus ladanifer*
2	Shrub	High	*Quercus pyrenaica* and *Q. ilex*
3	Herbaceous	Low	Different crops
4	Forest	High	*Q. pyrenaica*
5	Shrub	High	*C. ladanifer , Rosmarinus*
6	Forest	Low	*Q. pyrenaica* and *Q. broteroi*
7	Forest	High	*Q. suber*
8	Forest	High	*Pinus pinaster*
9	Dehesa	> 30	*Q. ilex*
10	Shrub	Low	*R. officmallis, E. umbellata*

[8], [9]. ρ_T changes for different values of IL, but after the topographic correction is carried out, ρ_H should remain constant for different values of IL. Third, the standard deviation (SD) for each class should be reduced [12], [15], [24], meaning a greater intraclass homogeneity has been achieved. Finally, the accuracy of a nonsupervised classification [9], [14], [24] may be used to check the improvements in class discrimination.

IV. RESULTS

A. Spectral Coherence After Changes

Table I summarizes the changes in spectral characteristics of TM bands after the application of the different algorithms. It is observed that the IL weighted by the IL_m and the smoothed C-corrections maintain better the mean of the original (after atmospheric correction) TM bands, whereas the Minnaert correction provides the worst results. In terms of the SD, the single C as well as the smoothed C-corrections performed the best rendering the least change, whereas the IL weighted by the IL_m provided the worst results.

TABLE III
REDUCTION IN SD, MEASURED IN PERCENT REFLECTANCE, FOR THE DIFFERENT VEGETATION CLASSES AFTER ATMOSPHERIC CORRECTION FOR EACH TM BAND AND ALSO FOR THE TOTAL SUM OF ALL BANDS. NEGATIVE VALUES APPEAR IN BOLD, WHICH ARE THOSE VEGETATION CLASSES WHERE THE SD INCREASES AFTER THE TOPOGRAPHIC CORRECTION. VEGETATION CLASSES REFER TO TABLE II

Class	TM1	TM2	TM3	TM4	TM5	TM7	Total improvement	Correction
1	0.18	0.27	0.31	**-0.48**	0.85	0.76	1.89	IL weigh.
1	**-0.16**	**-0.16**	**-0.16**	0.63	**-0.60**	**-0.87**	**-1.32**	Minnaert
1	0.09	0.06	0.05	0.20	0.21	0.15	0.76	C-correction
1	0.21	0.32	0.37	0.36	1.00	0.81	3.06	C-correction3
1	0.21	0.33	0.38	0.37	1.04	0.83	3.16	C-correction5
1	0.21	0.31	0.37	0.36	1.04	0.82	3.11	C-correction7
2	0.12	0.20	0.23	**-0.86**	0.71	0.51	0.91	IL weigh.
2	**-0.46**	**-0.50**	**-0.49**	0.82	**-1.90**	**-2.35**	**-4.88**	Minnaert
2	**-0.10**	**-0.46**	**-0.62**	0.21	**-0.49**	**-0.79**	**-2.25**	C-correction
2	0.12	0.19	0.23	0.41	0.85	0.44	2.24	C-correction3
2	0.12	0.22	0.24	0.44	0.94	0.49	2.45	C-correction5
2	0.12	0.21	0.24	0.44	0.94	0.47	2.42	C-correction7
3	0.19	0.26	0.35	0.40	0.77	0.67	2.64	IL weigh.
3	0.11	0.16	0.23	0.15	0.50	0.39	1.54	Minnaert
3	0.12	0.18	0.24	0.13	0.48	0.42	1.56	C-correction
3	0.08	0.14	0.17	0.15	0.37	0.31	1.22	C-correction3
3	0.07	0.09	0.12	0.13	0.31	0.24	0.96	C-correction5
3	0.06	0.07	0.09	0.12	0.26	0.18	0.79	C-correction7
4	**-0.01**	0.03	**-0.04**	**-1.58**	0.78	0.21	**-0.60**	IL weigh.
4	**-1.08**	**-1.16**	**-1.48**	0.47	**-2.79**	**-3.88**	**-9.91**	Minnaert
4	**-0.61**	**-2.25**	**-2.42**	**-0.02**	**-1.03**	**-1.99**	**-8.32**	C-correction
4	0.01	**-0.01**	**-0.08**	0.05	1.02	0.30	1.30	C-correction3
4	0.06	0.07	0.01	0.06	1.19	0.45	1.84	C-correction5
4	0.06	0.08	0.03	0.05	1.22	0.46	1.90	C-correction7
5	0.10	0.16	0.21	0.17	0.49	0.41	1.54	IL weigh.
5	0.03	0.08	0.10	0.19	0.06	**-0.06**	0.40	Minnaert
5	0.06	0.10	0.13	0.11	0.25	0.23	0.88	C-correction
5	0.04	0.08	0.11	0.15	0.33	0.26	0.97	C-correction3
5	0.02	0.06	0.09	0.16	0.30	0.22	0.84	C-correction5
5	0.01	0.04	0.06	0.14	0.27	0.19	0.71	C-correction7
6	**-0.04**	**-0.03**	**-0.08**	**-1.50**	**-0.32**	**-0.05**	**-2.02**	IL weigh.
6	**-2.04**	**-2.15**	**-2.68**	0.67	**-6.17**	**-7.81**	**-20.18**	Minnaert
6	**-1.47**	**-5.48**	**-6.83**	0.10	**-3.56**	**-5.00**	**-22.24**	C-correction
6	**-0.19**	**-0.39**	**-0.47**	0.23	**-0.20**	**-0.37**	**-1.38**	C-correction3
6	**-0.10**	**-0.21**	**-0.28**	0.25	0.17	**-0.02**	**-0.19**	C-correction5
6	**-0.08**	**-0.19**	**-0.24**	0.27	0.25	0.04	0.04	C-correction7
7	0.08	0.18	0.22	0.14	1.21	0.65	2.48	IL weigh.
7	**-0.27**	**-0.02**	**-0.01**	0.73	0.05	**-0.78**	**-0.31**	Minnaert
7	**-0.06**	**-0.06**	**-0.20**	0.50	0.63	0.01	0.82	C-correction
7	0.06	0.17	0.19	0.66	0.97	0.50	2.55	C-correction3
7	0.06	0.16	0.18	0.68	0.93	0.48	2.49	C-correction5
7	0.06	0.16	0.17	0.69	0.91	0.46	2.44	C-correction7
8	0.03	0.06	0.07	0.22	0.16	0.13	0.68	IL weigh.
8	**-0.09**	**-0.08**	**-0.11**	0.50	**-0.21**	**-0.31**	**-0.30**	Minnaert
8	**-0.03**	**-0.03**	**-0.06**	0.26	**-0.08**	**-0.13**	**-0.08**	C-correction
8	0.01	0.01	0.00	0.39	0.04	**-0.02**	0.43	C-correction3
8	0.00	0.01	0.00	0.41	0.05	**-0.03**	0.44	C-correction5
8	0.00	0.00	**-0.01**	0.42	0.03	**-0.03**	0.41	C-correction7
9	0.16	0.20	0.29	0.40	0.46	0.43	1.94	IL weigh.
9	0.15	0.19	0.27	0.10	0.30	0.35	1.35	Minnaert
9	0.12	0.18	0.25	0.09	0.25	0.29	1.18	C-correction
9	0.06	0.13	0.15	0.13	0.18	0.18	0.85	C-correction3
9	0.04	0.06	0.07	0.05	0.06	0.07	0.35	C-correction5
9	0.01	0.04	0.07	0.05	0.07	0.08	0.32	C-correction7
10	0.22	0.30	0.37	0.80	0.75	0.69	3.14	IL weigh.
10	0.25	0.31	0.37	0.32	0.62	0.72	2.60	Minnaert
10	0.21	0.32	0.39	0.24	0.56	0.61	2.33	C-correction
10	0.18	0.27	0.30	0.32	0.42	0.44	1.93	C-correction3
10	0.15	0.23	0.22	0.28	0.31	0.34	1.53	C-correction5
10	0.18	0.18	0.21	0.26	0.31	0.33	1.47	C-correction7

B. Class Homogeneity

The vegetation map was used to analyze the SD within each vegetation class. A total number of ten classes were chosen, where the topographic distortion was more evident. These classes cover 11.17% of the National Park's area and include the main vegetation types present (Table II). The result is shown in Table III. Most topographic correction methods implied a decrease in SD, meaning greater intraclass homogeneity. The Minnaert correction showed the worst results, which could be due to the implementation of the slope in the model. The smoothed C-correction 3, 5, and 7 and the IL weighted were the methods that better reduced the variability within each vegetation class. The C-correction was in between, failing mainly for classes 4 and 6, where IL conditions are very low, increasing the ρ_H excessively and consequently the SD.

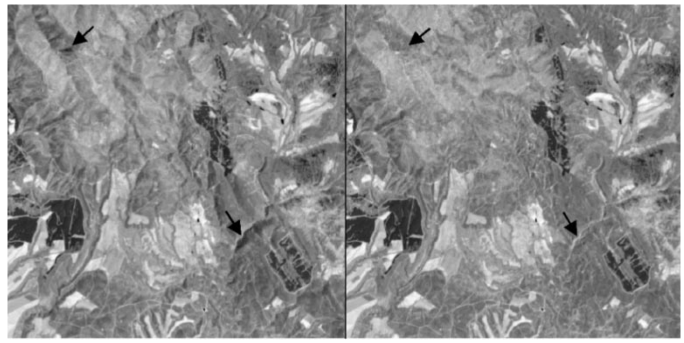

(a) (b)

Fig. 5. Northern Cabañeros National Park (a) before and (b) after carrying out the topographic correction. Arrows mark examples of areas were the topographic correction was efficient. False color composite (TM4–5-3) in grayscale, July 21st, 1997.

The smoothed C-corrections showed a better result as the smoothing factor was increased for classes were IL was very low (classes 4 and 6), but is was the other way around for the other classes.

V. CONCLUSION

Out of the different topographic corrections tested, the smoothed C-corrections retained best the spectral characteristics of each band and provided the highest reduction in class variability. The use of a smoothing factor of five (Fig. 5) allowed globally better results for all classes tested.

Further research should be done to test the different methods with other images of the same study area under worse illumination conditions (lower sun elevation angle) and on other study areas. All topographic correction methods tested assume the ρ_H is constant; that is to say, it has only one spectral class for homogeneous images. But there is a mixture of different vegetation classes in Mediterranean ecosystems. Some authors even say that it is impossible to perform a topographic correction without knowing the vegetation classes in advance [7], since the topographic effect is vegetation dependent [3]. It would be recommendable to perform this correction in order to avoid this risk. A smoothed correction does not alter reflectance values significantly, whereas a more extreme correction could introduce additional errors.

ACKNOWLEDGMENT

The authorities of the Cabañeros National Park helped in the fieldwork and kindly provided ancillary data. Linguistic assistance from P. Vaughan is also acknowledged.

REFERENCES

[1] P. M. Teillet, B. Guindon, and D. G. Goodeonugh, "On the slope-aspect correction of multispectral scanner data," *Can. J. Remote Sens.*, vol. 8, pp. 84–106, 1982.

[2] C. R. Duguay and E. F. LeDrew, "Estimating surface reflectance and albedo from Landsat-5 TM over rugged terrain," *Photogramm. Eng. Remote Sens.*, vol. 58, pp. 551–558, 1992.
[3] C. Leprieur, J. M. Durand, and J. L. Peyron, "Influence of topography on forest reflectance using Landsat Thematic Mapper and digital terrain data," *Photogramm. Eng. Remote Sens.*, vol. 54, pp. 491–496, 1988.
[4] T. Tokola, J. Sarkeala, and M. van der Linden, "Use of topographic correction in Landsat TM-based forest interpretation in Nepal," *Int. J. Remote Sens.*, vol. 22, pp. 551–563, 2001.
[5] F. W. Davis and S. Goetz, "Modeling vegetation pattern using digital terrain data," *Landscape Ecol.*, vol. 4, pp. 69–80, 1990.
[6] A. H. Strahler, "Stratification of natural vegetation for forest and rangeland inventory using Landsat digital imagery and collateral data," *Int. J. Remote Sens.*, vol. 2, pp. 15–41, 1981.
[7] A. G. Thomson and C. Jones, "Effects of topography on radiance from upland vegetation in North Wales," *Int. J. Remote Sens.*, vol. 11, pp. 829–840, 1990.
[8] S. Ekstrand, "Landsat -TM based forest damage assessment: Correction for topographic effects," *Photogramm. Eng. Remote Sens.*, vol. 62, pp. 151–161, 1996.
[9] P. Meyer, K. I. Itten, T. Kellenbenberger, S. Sandmeier, and R. Sandmeier, "Radiometric corrections of topographically induced effects on Landsat TM data in an alpine environment," *ISPRS J. Photogramm. Remote Sens.*, vol. 48, pp. 17–28, 1993.
[10] J. Jansa, "A global topographic normalization algorithm for satellite images," in *Proc. Int. Arch. Photogramm. Remote Sens.*, Budapest, Hungary, 1998.
[11] R. Richter, "Correction of atmospheric and topographic effects for high spatial resolution satellite imagery," *Int. J. Remote Sens.*, vol. 18, pp. 1099–1111, 1997.
[12] J. D. Colby, "Topographic normalization in rugged terrain," *Photogramm. Eng. Remote Sens.*, vol. 57, pp. 531–537, 1991.
[13] N. M. Short, *The Landsat Tutorial Workbook: Basics of Satellite Remote Sensing*. Washington, DC: NASA Scientific and Technical Information Branch, 1982.
[14] C. Conese, M. A. Gilabert, F. Maselli, and L. Bottai, "Topographic normalization of TM scenes through the use of an atmospheric correction method and digital terrain models," *Photogramm. Eng. Remote Sens.*, vol. 59, pp. 1745–1753, 1993.
[15] D. L. Civco, "Topographic normalization of Landsat Thematic Mapper digital imagery," *Photogramm. Eng. Remote Sens.*, vol. 55, pp. 1303–1309, 1989.
[16] B. Holben and C. Justice, "The topographic effect on spectral response from nadir pointing sources," *Photogramm. Eng. Remote Sens.*, vol. 46, pp. 1191–1200, 1980.
[17] S. R. Sandmeier and K. I. Itten, "A physically-based model to correct atmospheric and illumination effects in optical satellite data of rugged terrain," *IEEE Trans. Geosci. Remote Sensing*, vol. 35, pp. 708–717, May 1997.
[18] ——, "A field goniometer system (FIGOS) for acquisition of hyperspectral BRDF data," *IEEE Trans. Geosci. Remote Sensing*, vol. 37, pp. 978–986, Mar. 1999.
[19] M. Minnaert, "The reciprocity principle in lunar photometry," *Astrophys. J.*, vol. 93, pp. 403–410, 1941.
[20] L. Alonso, J. Breva, A. Caballero, I. Doadrio, J. A. Fernández, J. Jiménez, J. L. García, J. C. Gutiérrez, J. N. Guzmán, G. Olmedo, I. Rábano, M. A. San José, A. R. Del Valle, and J. Vaquero, *Parque Nacional de Cabañeros*, 1st ed., 1997, Ecohábitat.
[21] P. S. Chavez, "Image-based atmospheric corrections. Revisited and improved," *Photogramm. Eng. Remote Sens.*, vol. 62, pp. 1025–1036, 1996.
[22] M. A. Gilabert, C. Conese, and F. Maselli, "An atmospheric correction method for the automatic retrieval of surface reflectances from TM images," *Int. J. Remote Sens.*, vol. 15, pp. 2065–2086, 1994.
[23] A. Rosenfeld and J. Pfaltz, "Distance functions on digital pictures," *Pattern Recognit.*, vol. 1, pp. 33–61, 1968.
[24] X. Pons and L. Solé-Sugrañes, "A simple radiometric correction model to improve automatic mapping of vegetation from multispectral satellite data," *Remote Sens. Environ.*, vol. 48, pp. 191–204, 1994.
[25] E. Chuvieco, *Teledetección Ambiental*. Barcelona, Spain: Ariel, 2002.

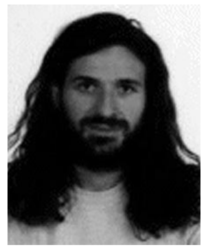

David Riaño received the Ph.D. degree in environmental sciences from the University of Alcalá, Madrid, Spain, in 2002.

He is currently a Postdoctoral Fulbright Scholar with the Center for Spatial Technologies and Remote Sensing, Department of Land, Air and Water Resources, University of California, Davis. His research interests are fuel type mapping and vegetation moisture content.

Emilio Chuvieco received the Ph.D. degree in geography from the University Complutense, Madrid, Spain, in 1985.

He is currently a Professor in the Department of Geography, University of Alcalá, Madrid, Spain. His research interests are vegetation moisture content, fuel type mapping, meteorological danger indexes, burned area mapping, fire danger, and human factors of fire risk.

Javier Salas received the Ph.D. degree in geography from the University of Alcalá, Madrid, Spain, in 1995.

He is currently an Associate Professor in the Department of Geography, University of Alcalá. His research interests are fuel type mapping and fire danger.

Inmaculada Aguado received the Ph.D. degree in geography from the University of Alcalá, Madrid, Spain, in 2001.

She is currently an Associate Professor in the Department of Geography, University of Alcalá. Her research interests are meteorological danger indexes and fire danger.